World Electric Vehicle Journal

MDPI

Article

Prescribed Performance Speed Control Without Initial Condition Restrictions for Asynchronous Motor Drive Systems

Ruibo Sun [1,2], Na Sang [3,*], Zhongyu Zhang [1], Shihang Hu [1], Zishuo Zhao [1] and Ye Zhang [1,4,*]

[1] Institute of Energy Supply Technology for High-End Equipment, Jiangsu Key Laboratory of Atmospheric Environment Monitoring and Pollution Control, Jiangsu Collaborative Innovation Center of Atmospheric Environment and Equipment Technology, School of Environmental Science and Engineering, Nanjing University of Information Science & Technology, Nanjing 210044, China; ruibosun@foxmail.com (R.S.); 202213380021@nuist.edu.cn (Z.Z.); shihanghu99@gmail.com (S.H.); zhao_zishuo2002@163.com (Z.Z.)

[2] School of Electrons and Information Engineering, University of Science and Technology Liaoning, Anshan 114051, China

[3] School of Electromechanical and Transit, Zhejiang Fashion Institute of Technology, Ningbo 315211, China

[4] Sinopec Yangzi Petrochemical Co., Ltd., Nanjing 210048, China

* Correspondence: 2025700031@zjff.edu.cn (N.S.); zhangye.yzsh@sinopec.com (Y.Z.)

Abstract

Asynchronous motors are widely used in electric vehicle drive systems because of their simple structure, low cost, and high reliability. Accurate speed tracking and smooth transient response are important during start-up, acceleration, and deceleration. However, sensing uncertainties and sensor faults may affect the measured signals and reduce control performance. In this study, an adaptive prescribed performance control (PPC) method is developed for asynchronous motor speed regulation. A nonlinear mapping and an improved tangent-type barrier Lyapunov function (BLF) are used to remove the requirement that the initial tracking error must lie within the prescribed performance bounds. Radial basis function neural networks are used to approximate the unknown nonlinear terms. The stability analysis shows that all closed-loop signals remain bounded and that the tracking error enters and remains within the prescribed performance region after the initial expansion stage. Simulations under different initial motor speeds, the considered sensor-fault conditions, and load disturbances are conducted. Under the adopted comparative conditions, the proposed method reduces the convergence time, steady-state error, maximum tracking error, and recovery time by 69.5%, 93.4%, 92.2%, and 49.4%, respectively. The results show that the proposed method improves the transient response, tracking accuracy, and disturbance recovery of the asynchronous motor drive system.

Keywords: asynchronous motor; prescribed performance control (PPC); barrier Lyapunov function (BLF); adaptive control

Check for updates

Academic Editor: Joeri Van Mierlo

Received: 31 May 2026
Revised: 22 July 2026
Accepted: 27 July 2026
Published: 1 August 2026

1. Introduction

Asynchronous motors are widely used in electric vehicle drive systems [1,2]. In electric vehicle applications, the drive motor is required to achieve accurate speed tracking and smooth transient response during start-up, acceleration, and deceleration. Therefore, developing advanced speed control methods for asynchronous motors is important for improving the dynamic performance of electric vehicle drive systems.

Extensive research on the control of asynchronous motors has primarily focused on achieving rapid adjustment and high-accuracy speed tracking [3–5]. In Ref. [6], fractional-order dynamics were introduced into a motor system with an internal proportional–integral–derivative (PID) controller. However, the nonlinear characteristics of the motor degraded the performance of the PID controller, resulting in a long settling time. To reduce the settling time, sliding mode control (SMC) has been widely investigated. In Ref. [7], a hybrid control scheme combining SMC with fuzzy logic control was proposed to improve field-oriented control performance. A fast integral terminal sliding-mode surface was proposed in Ref. [8]. However, the high-frequency switching inherent in SMC may cause chattering in the control input and lead to undesirable mechanical wear. To improve the disturbance rejection capability of motor control systems, a nonsingular fast terminal SMC strategy was developed in Ref. [9]. Although these methods improve tracking accuracy and disturbance rejection, transient requirements such as tracking-error peak and convergence speed are not always explicitly guaranteed.

To improve transient performance, prescribed performance control (PPC) has been introduced for asynchronous motor control [10–12]. PPC constrains the tracking error within predefined performance bounds and thus provides a direct way to regulate transient and steady-state performance. A predefined-time control method with prescribed performance was proposed in Ref. [13], and an error-transformation-based adaptive PPC method was applied to asynchronous motors in Ref. [14]. Nevertheless, the non-smooth terms used in these control laws may induce chattering. To address this problem, a fixed-time PPC method based on adaptive observers was proposed in Ref. [15], which ensures rapid convergence and prescribed performance within a predetermined time. However, the error transformation used in this controller may introduce singularity problems.

To avoid the singularities associated with error transformation, the barrier Lyapunov function (BLF) has been introduced into PPC design [16–19]. BLF-based methods can directly constrain the tracking error without requiring an inverse error transformation. However, most existing BLF-based PPC methods assume that the initial tracking error is located within the predefined performance bounds. This requirement restricts the selection of the prescribed performance function and limits the applicable initial operating range of the motor. To remove this restriction, a nonlinear mapping method was proposed in Ref. [20]. This method allows the prescribed performance function to be selected independently of the initial value of the constrained variable, thereby eliminating its dependence on the initial condition. However, the conclusions in Ref. [20] were mainly developed for a relatively simple system, and their extension to the multi-input–multi-output nonlinear dynamics of asynchronous motors requires further investigation.

In practical motor drive systems, currents and rotor speed are obtained from sensors or state observers. Sensing uncertainties and sensor faults may reduce the accuracy of the measured signals and degrade the control performance [21,22]. Sensor fault modeling and related control methods have therefore been investigated in Refs. [23,24]. In particular, inaccurate speed measurements may result in a large measured tracking error. This motivates the development of a PPC method for asynchronous motors that can guarantee transient performance without requiring the initial speed tracking error to satisfy predefined bounds.

Motivated by the above discussion, this study investigates a PPC strategy that is independent of the initial motor speed for asynchronous motor systems. An adaptive PPC method is developed, in which a nonlinear mapping is used to remove the initial-condition restriction, and an improved tangent-type BLF is employed to constrain the tracking error and guarantee the boundedness of all closed-loop signals. The main contributions of this study are summarized as follows:

- The present work generalizes the conclusions of Ref. [20] to a multi-input–multi-output system.
- In contrast to the methods in Refs. [14,15], the proposed controller does not require the initial speed tracking error to lie within the prescribed performance bounds. The

Lyapunov analysis guarantees the boundedness of all closed-loop signals and ensures that the tracking error enters and remains within the prescribed performance region after the initial expansion stage.

The remainder of this paper is organized as follows: Section 2 describes the system and preliminaries; Section 3 discusses the controller design and stability analysis; Section 4 provides the simulation results; and Section 5 concludes this study.

2. Plant Formulation and Preliminaries

2.1. Plant Formulation

The asynchronous motor model uses the synchronous rotating d-q reference frame. In this frame, the q-axis current i_q mainly affects electromagnetic torque, whereas the d-axis current i_d regulates rotor flux. The symbols ψ_d and ω denote the rotor flux linkage and rotor angular velocity, respectively. The following equations describe the motor dynamics [19]:

$$\begin{cases} \dfrac{d\omega}{dt} = \dfrac{n_p L_m}{L_r J}\psi_d i_q - \dfrac{T_L}{J}, \\ \dfrac{di_q}{dt} = -\dfrac{L_m^2 R_r + L_r^2 R_s}{\sigma L_s L_r^2} i_q - \dfrac{L_m n_p}{\sigma L_s L_r}\omega\psi_d - n_p\omega i_d - \dfrac{L_m R_r}{L_r}\dfrac{i_q i_d}{\psi_d} + \dfrac{1}{\sigma L_s}u_q, \\ \dfrac{d\psi_d}{dt} = -\dfrac{R_r}{L_r}\psi_d + \dfrac{L_m R_r}{L_r} i_d, \\ \dfrac{di_d}{dt} = -\dfrac{L_m^2 R_r + L_r^2 R_s}{\sigma L_s L_r^2} i_d + \dfrac{L_m R_r}{\sigma L_s L_r^2}\psi_d + n_p\omega i_q + \dfrac{L_m R_r}{L_r}\dfrac{i_q^2}{\psi_d} + \dfrac{1}{\sigma L_s}u_d. \end{cases} \tag{1}$$

where n_p, T_L, and L_m denote the number of pole pairs, load torque, and mutual inductance, respectively. J denotes the moment of inertia; ω and ψ_d represent the angular velocity and rotor flux linkage of the rotor, respectively; i_d, i_q, u_d, and u_q are the currents and voltages in the d-q reference frame; L_s and L_r denote the inductances of the stator and rotor, respectively; and R_s and R_r are the resistances of the stator and rotor, respectively. In addition, define the leakage coefficient as $\sigma = 1 - L_m^2/(L_s L_r)$.

The rotor-flux, d-axis-current, and q-axis-current terms describe the coupling between the mechanical speed and the electrical variables. The reciprocal rotor-flux terms come from the field-oriented induction motor model. During normal field-oriented operation, the rotor flux remains positive; assuming that it stays bounded away from zero keeps the model well defined.

For a compact controller design, the following state variables and coefficients are introduced. Set the compact notations as $x_1 = \omega$, $x_2 = i_q$, $x_3 = \psi_d$, and $x_4 = i_d$. In addition, define

$$b_0 = \frac{n_p L_m}{L_r}, \quad b_1 = -\frac{L_m^2 R_r + L_r^2 R_s}{\sigma L_s L_r^2}, \quad b_2 = -\frac{L_m n_p}{\sigma L_s L_r}, \quad b_3 = n_p,$$
$$b_4 = \frac{L_m R_r}{L_r}, \quad b_5 = \frac{1}{\sigma L_s}, \quad d_0 = -\frac{R_r}{L_r}, \quad d_2 = \frac{L_m R_r}{\sigma L_s L_r^2}.$$

These substitutions yield a compact state-space model while preserving the physical meaning of the motor variables. Here, the definitions $x_1 = \omega$, $x_2 = i_q$, $x_3 = \psi_d$, and $x_4 = i_d$ show that the state variables represent the motor speed, the torque-producing current, the rotor flux linkage, and the flux-producing current, respectively.

The motor model then takes the form

$$\begin{cases} \dot{x}_1 = x_2 + F_1, \\ \dot{x}_2 = x_3 + F_2 + b_5 u_q, \\ \dot{x}_3 = x_4 + F_3, \\ \dot{x}_4 = x_4 + F_4 + b_5 u_d, \\ y = x_1. \end{cases} \tag{2}$$

where

$$\begin{aligned} F_1 &= \frac{b_0}{J} x_2 x_3 - x_2 - \frac{T_L}{J}, \\ F_2 &= b_1 x_2 + b_2 x_1 x_3 - b_3 x_1 x_4 - b_4 \frac{x_2 x_4}{x_3} - x_3, \\ F_3 &= d_0 x_3 + b_4 x_4 - x_4, \\ F_4 &= b_1 x_4 + d_2 x_3 + b_3 x_1 x_2 + b_4 \frac{x_2^2}{x_3} - x_4. \end{aligned}$$

By adding and subtracting appropriate state terms, the motor model can be rewritten in the following strict-feedback-like form. The nonlinear functions therefore collect the motor coupling terms, load effect, and electrical–mechanical interaction terms.

Let y_r denote the desired speed trajectory. The tracking error becomes

$$e_1 = y - y_r. \tag{3}$$

The control objective is to design the voltage inputs such that the speed tracking error converges within the prescribed performance bound, while all closed-loop signals remain bounded.

2.2. Preliminaries

Before presenting the prescribed performance controller, two standard tools are introduced. They will be used in the adaptive approximation and Lyapunov analysis.

Lemma 1 (See [23])**.** *The radial basis function neural network (RBFNN) can approximate an unknown smooth nonlinear function $f(Z) : \mathbb{R}^q \to \mathbb{R}$ defined on a compact set as follows:*

$$f(Z) = W^{*\mathrm{T}} S(Z) + \delta(Z), \tag{4}$$

where $W^{*\mathrm{T}}$ denotes the optimal weight vector defined as

$$W^* = \arg \min_{W \in \mathbb{R}^\iota} \left\{ \sup_{Z \in \Omega} \left| f(Z) - W^{\mathrm{T}} S(Z) \right| \right\},$$

$\delta(Z)$ is the approximation error satisfying $|\delta| \le \varepsilon$, and ε is an unknown positive constant. $S(Z) = [S_1(Z), S_2(Z), S_3(Z), \ldots, S_\iota(Z)]^{\mathrm{T}}$ is a known smooth vector function with $\iota > 1$ neural-network nodes. The basis function $S_i(Z)$, $i = 1, 2, \ldots, \iota$, is chosen as a Gaussian function of the form

$$S_i(Z) = \exp\left(- \frac{\|Z - \mu_i\|^2}{(o_i)^2} \right), \quad i = 1, 2, 3, \ldots, \iota. \tag{5}$$

Here, o_i is the width of the Gaussian function and $\mu_i = [\mu_{i,1}, \mu_{i,2}, \mu_{i,3}, \ldots, \mu_{i,q}]^{\mathrm{T}}$ is the center of the receptive field.

In this study, the RBFNN is used to approximate the unknown nonlinear functions generated by the motor coupling terms and the backstepping design. These nonlinear functions are related to the compact functions defined above. Thus, the RBFNN helps compensate for model uncertainty, load variation, and unmodeled nonlinear dynamics.

Lemma 2 (See [15])**.** *For any $x, y \in \mathbb{R}^2$, the following inequality holds:*

$$xy \leq \frac{\delta^p}{p}|x|^p + \frac{1}{q\delta^q}|y|^q, \tag{6}$$

where $\delta > 0$, $p > 1$, $q > 1$, and $(p-1)(q-1) = 1$.

This inequality is used to deal with the cross terms in the derivative of the Lyapunov function. In the motor control problem, such cross terms are caused by the coupling between speed, current, rotor flux, and neural-network approximation errors.

2.3. PPC-Based Speed Control

The purpose of prescribed performance control is to constrain the tracking error within a predefined time-varying boundary. For the speed tracking error $e_1 = y - y_r$, the desired prescribed performance condition is

$$-\rho(t) < e_1(t) < \rho(t), \tag{7}$$

where $\rho(t)$ is the prescribed performance function, which is defined as follows:

$$\rho(t) = \begin{cases} \rho_0\left(1 - \dfrac{t}{T_a}\right)\exp\left(1 - \dfrac{T_a}{T_a - t}\right) + \rho_\infty, & t < T_a, \\ \rho_\infty, & t \geq T_a. \end{cases} \tag{8}$$

Here, ρ_0 determines the initial width of the performance bound, ρ_∞ determines the final steady-state error bound, and T_a is the prescribed settling time. A smaller ρ_∞ gives a higher steady-state tracking accuracy, while T_a reflects the expected convergence speed.

Conventional PPC methods usually require the initial tracking error to satisfy the prescribed performance bound at the initial time. This condition is restrictive for electric vehicle drive systems because the initial speed may vary under different driving conditions. In addition, sensing noise or sensor faults may make the measured initial speed different from the actual motor speed. To relax this restriction, the following nonlinear mapping is introduced:

$$\lambda(e_1(t)) = \tanh(e_1(t)) = \frac{\exp(e_1(t)) - \exp(-e_1(t))}{\exp(e_1(t)) + \exp(-e_1(t))}. \tag{9}$$

For notational simplicity, let $\lambda(t) = \lambda(e_1(t))$. Its derivative with respect to e_1 is

$$\lambda_{e_1} = \frac{\partial \lambda}{\partial e_1} = 1 - \lambda^2(t) > 0. \tag{10}$$

Remark 1. *The mapping function $\tanh(\cdot) \in (-1, 1)$ is strictly increasing. Therefore, the prescribed-performance constraint can be transformed as follows:*

$$\lambda(-\rho(t)) < \lambda(e_1(t)) < \lambda(\rho(t)). \tag{11}$$

Since the nonlinear mapping is smooth and strictly increasing, a large tracking error can be mapped into a bounded interval. This property allows the controller to handle a large initial tracking error without directly imposing the original performance boundary at the initial time.

To describe the initial expansion stage, consider an indirect constraint function $\varpi(t) = v(t)/\omega_0 + \lambda(\rho(t))$, where $v(t)$ denotes the smooth function

$$v(t) = \begin{cases} \left(\omega_0 - \dfrac{t}{T_f}\right) \exp\left(1 - \dfrac{T_f}{T_f - t}\right), & t < T_f, \\ 0, \quad t \geq T_f. \end{cases} \tag{12}$$

where $\omega_0 > 0$ is a design constant, T_f represents the time at which the constrained variable enters the prescribed performance region, and $v(t)$ is the initial expansion function.

Remark 2. *The initial expansion should be completed before the prescribed settling time. Thus, the time parameters should be chosen such that* $T_f < T_a$.

At the initial time, $v(0) = \omega_0$, and hence

$$\varpi(0) = 1 + \lambda(\rho(0)) > 1. \tag{13}$$

For any finite initial tracking error, $|\lambda(e_1(0))| = |\tanh(e_1(0))| < 1$. Therefore,

$$|\lambda(e_1(0))| < \varpi(0), \tag{14}$$

which shows that the transformed constraint is initially feasible without requiring $|e_1(0)| < \rho(0)$. During the initial expansion stage, the transformed constraint is defined as

$$-\varpi(t) < \lambda(t) < \varpi(t). \tag{15}$$

The indirect constraint enlarges the feasible region during the initial transient and then gradually recovers the prescribed bound. For $t \geq T_f$, $v(t) = 0$ and $\varpi(t) = \lambda(\rho(t))$. Consequently, maintaining the transformed constraint implies

$$|\lambda(e_1(t))| < \lambda(\rho(t)), \qquad t \geq T_f. \tag{16}$$

Because $\tanh(\cdot)$ is odd and strictly increasing, the above inequality is equivalent to

$$|e_1(t)| < \rho(t), \qquad t \geq T_f. \tag{17}$$

Thus, the proposed PPC design does not require the initial motor speed to satisfy the original prescribed performance constraint.

3. Prescribed Performance Controller Design and Stability Analysis

3.1. Controller Design

The controller is designed through a Lyapunov-based recursive procedure based on the strict-feedback-like model obtained in Section 2. In each step, a Lyapunov function is selected for the current error variable, and its derivative is calculated. The virtual control law or actual control input is designed from this derivative to construct the main negative feedback term, while the adaptive law handles the RBFNN approximation term and keeps the parameter-estimation-related term bounded. Thus, each Lyapunov derivative can be arranged as negative terms, next-step coupling terms, and bounded residual terms.

To construct the controller and adaptive laws, the following coordinate transformation is introduced:

$$\begin{cases} \xi_1 = \tan\left(\dfrac{\pi\lambda}{2\varpi}\right), \\ \xi_i = x_i - \alpha_{i-1}, \quad i = 2, 3, 4. \end{cases} \tag{18}$$

Define the positive time-varying coefficient

$$R = \frac{\pi(1+\xi_1^2)}{2\varpi}\lambda_{e_1} > 0. \tag{19}$$

For $i = 1,2,3,4$, define

$$\theta_i = \|W_i^*\|^2, \qquad \tilde{\theta}_i = \theta_i - \hat{\theta}_i,$$

where $c_i, a_i, r_i, \tau_i > 0$ are design parameters. In addition, $\alpha_2 = y_d$, where y_d denotes the desired rotor-flux trajectory.

In this transformation, ξ_1 is the transformed speed tracking error, while ξ_2, ξ_3, and ξ_4 are the error variables introduced for the backstepping design. Since the tangent function tends to infinity near the boundary, the boundedness of ξ_1 implies that the transformed tracking error does not violate the prescribed performance constraint.

The following design proceeds in four recursive steps. Step 1 treats ξ_1 and leaves the ξ_2 coupling term. Step 2 treats ξ_2 and leaves the ξ_3 coupling term. Step 3 treats ξ_3 and leaves the ξ_4 coupling term. Step 4 treats ξ_4 and completes the Lyapunov construction.

Step 1: A Lyapunov function is chosen as

$$V_1 = \frac{1}{2}\xi_1^2 + \frac{1}{2r_1}\tilde{\theta}_1^2. \tag{20}$$

From $e_1 = x_1 - y_r$, $\dot{x}_1 = x_2 + F_1$, and $x_2 = \xi_2 + \alpha_1$, it follows that

$$\dot{\lambda} = \lambda_{e_1}\dot{e}_1 = \lambda_{e_1}(\xi_2 + \alpha_1 + F_1 - \dot{y}_r). \tag{21}$$

Differentiating $\xi_1 = \tan(\pi\lambda/(2\varpi))$ gives

$$\begin{aligned} \dot{\xi}_1 &= \sec^2\left(\frac{\pi\lambda}{2\varpi}\right)\frac{\pi}{2\varpi}\left(\dot{\lambda} - \frac{\lambda\dot{\varpi}}{\varpi}\right) \\ &= R\left(\alpha_1 + \xi_2 + F_1 - \dot{y}_r - \frac{\lambda\dot{\varpi}}{\varpi\lambda_{e_1}}\right). \end{aligned} \tag{22}$$

Therefore, the derivative of V_1 is

$$\dot{V}_1 = \xi_1\big(R\alpha_1 + \xi_2 + \bar{f}_1(Z_1)\big) - \frac{1}{r_1}\tilde{\theta}_1\dot{\hat{\theta}}_1, \tag{23}$$

where the unknown nonlinear function is defined as

$$\bar{f}_1(Z_1) = R\left(\xi_2 + F_1 - \dot{y}_r - \frac{\lambda\dot{\varpi}}{\varpi\lambda_{e_1}}\right) - \xi_2. \tag{24}$$

An RBFNN function

$$\bar{f}_1(Z_1) = W_1^{*\mathrm{T}}S_1(Z_1) + \delta_1(Z_1), \qquad |\delta_1(Z_1)| \le \varepsilon_1, \tag{25}$$

is applied to approximate $\bar{f}_1(Z_1)$, where

$$Z_1 = [x_1, x_2, x_3, x_4, \xi_1, \dot{y}_r, \varpi, \dot{\varpi}]^{\mathrm{T}}. \tag{26}$$

Using Young's inequality, we have

$$\begin{aligned}\xi_1\bar{f}_1(Z_1) &= \xi_1 W_1^{*\mathrm{T}} S_1 + \xi_1\delta_1 \\ &\le \frac{1}{2a_1^2}\xi_1^2\|W_1^*\|^2 S_1^{\mathrm{T}} S_1 + \frac{a_1^2}{2} + \frac{1}{2}\xi_1^2 + \frac{1}{2}\varepsilon_1^2 \\ &= \frac{1}{2a_1^2}\xi_1^2\theta_1 S_1^{\mathrm{T}} S_1 + \frac{a_1^2}{2} + \frac{1}{2}\xi_1^2 + \frac{1}{2}\varepsilon_1^2.\end{aligned} \tag{27}$$

The virtual control law and adaptive law are defined as

$$\alpha_1 = -\frac{1}{R}\left(\frac{1}{2a_1^2}\hat{\theta}_1 S_1^{\mathrm{T}} S_1 + c_1 + 1\right)\xi_1, \tag{28}$$

$$\dot{\hat{\theta}}_1 = \frac{r_1}{2a_1^2}\xi_1^2 S_1^{\mathrm{T}} S_1 - \tau_1\hat{\theta}_1, \tag{29}$$

where c_i, a_i, r_i, τ_i are positive design parameters.

The factor $1/R$ in the virtual control law compensates for the coefficient generated by differentiating the tangent transformation. The adaptive law is selected to cancel the parameter-estimation term in the Lyapunov derivative. Using $\xi_1\xi_2 \le \frac{1}{2}\xi_1^2 + \frac{1}{2}\xi_2^2$ and substituting the above expressions yields

$$\dot{V}_1 \le -c_1\xi_1^2 + \frac{1}{2}\xi_2^2 + \frac{a_1^2}{2} + \frac{1}{2}\varepsilon_1^2 + \frac{\tau_1}{r_1}\tilde{\theta}_1\hat{\theta}_1. \tag{30}$$

After Step 1, the remaining coupling term in ξ_2 is carried into the next Lyapunov derivative. Step 2 selects V_2 for ξ_2 and designs the actual input and adaptive law according to $\dot{V}_2$, so that the ξ_2 term is made negative while the next coupling term in ξ_3 is isolated.

Step 2: Define the Lyapunov function V_2 as

$$V_2 = \frac{1}{2}\xi_2^2 + \frac{1}{2r_2}\tilde{\theta}_2^2. \tag{31}$$

The derivative of V_2 is given by

$$\dot{V}_2 = \xi_2(\xi_3 + F_2 + y_d + b_5 u_q - \dot{\alpha}_1) - \frac{1}{r_2}\tilde{\theta}_2\dot{\hat{\theta}}_2 \tag{32}$$

An RBFNN function

$$\bar{f}_2(Z_2) = W_2^{*\mathrm{T}} S_2(Z_2) + \delta_2(Z_2), \qquad |\delta_2(Z_2)| \le \varepsilon_2, \tag{33}$$

is applied to approximate the following function:

$$\bar{f}_2(Z_2) = F_2 + y_d - \dot{\alpha}_1 \tag{34}$$

where

$$Z_2 = \left[x_1, x_2, x_3, x_4, \xi_1, \xi_2, \hat{\theta}_1, \dot{y}_r, \ddot{y}_r, y_d\right]^{\mathrm{T}} \tag{35}$$

Using Young's inequality, we have

$$\begin{aligned}\xi_2\bar{f}_2(Z_2) &= \xi_2 W_2^{*\mathrm{T}} S_2 + \xi_2\delta_2 \\ &\le \frac{1}{2a_2^2}\xi_2^2\|W_2^*\|^2 S_2^{\mathrm{T}} S_2 + \frac{a_2^2}{2} + \frac{1}{2}\xi_2^2 + \frac{1}{2}\varepsilon_2^2 \\ &= \frac{1}{2a_2^2}\xi_2^2\theta_2 S_2^{\mathrm{T}} S_2 + \frac{a_2^2}{2} + \frac{1}{2}\xi_2^2 + \frac{1}{2}\varepsilon_2^2.\end{aligned} \tag{36}$$

Similarly, the actual control input u_q and the adaptive law are defined as

$$u_q = -\frac{1}{b_5}\left(\frac{1}{2a_2^2}\hat{\theta}_2\xi_2 S_2^{\mathrm{T}} S_2 + \left(c_2 + \frac{3}{2}\right)\xi_2\right) \tag{37}$$

$$\dot{\hat{\theta}}_2 = \frac{r_2}{2a_2^2}\xi_2^2 S_2^{\mathrm{T}} S_2 - \tau_2\hat{\theta}_2 \tag{38}$$

Using $\xi_2\xi_3 \leq \frac{1}{2}\xi_2^2 + \frac{1}{2}\xi_3^2$ and substituting the actual control input and adaptive law gives

$$\dot{V}_2 \leq -c_2\xi_2^2 + \frac{1}{2}\xi_3^2 - \frac{1}{2}\xi_2^2 + \frac{a_2^2}{2} + \frac{1}{2}\varepsilon_2^2 + \frac{\tau_2}{r_2}\tilde{\theta}_2\hat{\theta}_2 \tag{39}$$

After Step 2, $\dot{V}_2$ has the same recursive form: negative terms in ξ_2, a coupling term in ξ_3, and a bounded residual term. Step 3 selects V_3 for ξ_3 and designs the virtual control law and adaptive law according to $\dot{V}_3$, so that the remaining coupling is shifted to ξ_4.

Step 3: Consider the following Lyapunov function candidate:

$$V_3 = \frac{1}{2}\xi_3^2 + \frac{1}{2r_3}\tilde{\theta}_3^2, \tag{40}$$

The derivative of V_3 is given by

$$\dot{V}_3 = \xi_3(\xi_4 + F_3 - \dot{y}_d + \alpha_3) - \frac{1}{r_3}\tilde{\theta}_3\dot{\hat{\theta}}_3 \tag{41}$$

An RBFNN function $\bar{f}_3(Z_3) = W_3^{*\mathrm{T}} S_3(Z_3) + \delta_3(Z_3)$, $|\delta_3(Z_3)| \leq \varepsilon_3$ is applied to approximate the following function:

$$\bar{f}_3(Z_3) = F_3 - \dot{y}_d \tag{42}$$

where

$$Z_3 = \left[x_1, x_2, x_3, x_4, \xi_1, \xi_2, \xi_3, \hat{\theta}_1, \hat{\theta}_2, \dot{y}_r, \ddot{y}_r, y_d, \dot{y}_d\right]^{\mathrm{T}} \tag{43}$$

Based on Young's inequality, we have

$$\begin{aligned}
\xi_3\bar{f}_3(Z_3) &= \xi_3 W_3^{*\mathrm{T}} S_3 + \xi_3\delta_3 \\
&\leq \frac{1}{2a_3^2}\xi_3^2\|W_3^*\|^2 S_3^{\mathrm{T}} S_3 + \frac{a_3^2}{2} + \frac{1}{2}\xi_3^2 + \frac{1}{2}\varepsilon_3^2 \\
&= \frac{1}{2a_3^2}\xi_3^2\theta_3 S_3^{\mathrm{T}} S_3 + \frac{a_3^2}{2} + \frac{1}{2}\xi_3^2 + \frac{1}{2}\varepsilon_3^2.
\end{aligned} \tag{44}$$

By analogy, the virtual control law α_3 and adaptive law $\hat{\theta}_3$ are designed as

$$\alpha_3 = -\left(\frac{1}{2a_3^2}\hat{\theta}_3 S_3^{\mathrm{T}} S_3\xi_3 + \left(c_3 + \frac{3}{2}\right)\xi_3\right), \tag{45}$$

$$\dot{\hat{\theta}}_3 = \frac{r_3}{2a_3^2}\xi_3^2 S_3^{\mathrm{T}} S_3 - \tau_3\hat{\theta}_3. \tag{46}$$

Using $\xi_3\xi_4 \leq \frac{1}{2}\xi_3^2 + \frac{1}{2}\xi_4^2$ and substituting the above expressions yields

$$\dot{V}_3 \leq -c_3\xi_3^2 + \frac{1}{2}\xi_4^2 - \frac{1}{2}\xi_3^2 + \frac{a_3^2}{2} + \frac{1}{2}\varepsilon_3^2 + \frac{\tau_3}{r_3}\tilde{\theta}_3\hat{\theta}_3 \tag{47}$$

After Step 3, $\dot{V}_3$ contains negative terms in ξ_3, a coupling term in ξ_4, and a bounded residual term. Step 4 handles this final coupling term through the last Lyapunov derivative. Since no further error variable is introduced, the recursive stability construction is completed in this step.

Step 4: Define Lyapunov function V_4 as follows:

$$V_4 = \frac{1}{2}\xi_4^2 + \frac{1}{2r_4}\tilde{\theta}_4^2, \tag{48}$$

The derivative of V_4 is given by

$$\dot{V}_4 = \xi_4(x_4 + F_4 + b_5 u_d - \dot{\alpha}_3) - \frac{1}{r_4}\tilde{\theta}_4\dot{\hat{\theta}}_4 \tag{49}$$

An RBFNN function

$$\bar{f}_4(Z_4) = W_4^{*\mathrm{T}} S_4(Z_4) + \delta_4(Z_4) \tag{50}$$

$$|\delta_4(Z_4)| \leq \varepsilon_4 \tag{51}$$

is applied to approximate $\bar{f}_4(Z_4) = x_4 + F_4 - \dot{\alpha}_3$, where

$$Z_4 = \left[x_1, x_2, x_3, x_4, \xi_1, \xi_2, \xi_3, \xi_4, \hat{\theta}_1, \hat{\theta}_2, \hat{\theta}_3, \dot{y}_r, \ddot{y}_r, y_d, \dot{y}_d\right]^{\mathrm{T}}.$$

Based on Young's inequality, we have

$$\begin{aligned}
\xi_4 \bar{f}_4(Z_4) &= \xi_4 W_4^{*\mathrm{T}} S_4 + \xi_4 \delta_4 \\
&\leq \frac{1}{2a_4^2}\xi_4^2 \|W_4^*\|^2 S_4^{\mathrm{T}} S_4 + \frac{a_4^2}{2} + \frac{1}{2}\xi_4^2 + \frac{1}{2}\varepsilon_4^2 \\
&= \frac{1}{2a_4^2}\xi_4^2 \theta_4 S_4^{\mathrm{T}} S_4 + \frac{a_4^2}{2} + \frac{1}{2}\xi_4^2 + \frac{1}{2}\varepsilon_4^2.
\end{aligned} \tag{52}$$

Analogous results can be obtained stating that the control law u_d and adaptive law $\hat{\theta}_4$ are defined as

$$u_d = -\frac{1}{b_5}\left(\frac{1}{2a_4^2}\hat{\theta}_4 S_4^{\mathrm{T}} S_4 \xi_4 + (c_4 + 1)\xi_4\right) \tag{53}$$

$$\dot{\hat{\theta}}_4 = \frac{r_4}{2a_4^2}\xi_4^2 S_4^{\mathrm{T}} S_4 - \tau_4 \hat{\theta}_4. \tag{54}$$

Substituting the above expressions gives

$$\dot{V}_4 \leq -c_4\xi_4^2 - \frac{1}{2}\xi_4^2 + \frac{a_4^2}{2} + \frac{1}{2}\varepsilon_4^2 + \frac{\tau_4}{r_4}\tilde{\theta}_4\hat{\theta}_4 \tag{55}$$

3.2. Stability Analysis

The main result of this paper is presented in the following theorem.

Theorem 1. *Consider the asynchronous motor system (1). Assume that the reference signals y_r and y_d, together with their derivatives required in the controller, are bounded, and that the rotor flux x_3 remains bounded away from zero. If the proposed virtual control laws, actual control inputs, and adaptive laws are applied, then*

- *All signals in the closed-loop system are bounded;*
- *The speed tracking error*
  e_1 enters the prescribed performance region after the initial expansion stage and remains within it.

Proof of Theorem 1. Define the Lyapunov function of the motor system as □

$$V = \sum_{i=1}^{4} V_i \tag{56}$$

From the four recursive Lyapunov derivative inequalities, the following inequality is obtained:

$$\dot{V} \leq -\sum_{i=1}^{4} c_i \tilde{\xi}_i^2 + \sum_{i=1}^{4} \frac{\tau_i}{r_i} \tilde{\theta}_i \hat{\theta}_i + \sum_{i=1}^{4} \left(\frac{a_i^2}{2} + \frac{\varepsilon_i^2}{2} \right). \tag{57}$$

where the parameter-estimation cross term is bounded as

$$\frac{\tau_i}{r_i} \tilde{\theta}_i \hat{\theta}_i = \frac{\tau_i}{r_i} \tilde{\theta}_i (\theta_i - \tilde{\theta}_i) \leq \frac{\tau_i}{2r_i} \theta_i^2 - \frac{\tau_i}{2r_i} \tilde{\theta}_i^2, \tag{58}$$

and therefore

$$\begin{aligned} &\dot{V} \leq -pV + q, \\ &p = \min\{2c_1, 2c_2, 2c_3, 2c_4, \tau_1, \tau_2, \tau_3, \tau_4\}, \\ &q = \sum_{i=1}^{4} \left(\frac{a_i^2 + \varepsilon_i^2}{2} + \frac{\tau_i}{2r_i} \theta_i^2 \right). \end{aligned} \tag{59}$$

Since $p > 0$ and $q > 0$, inequality (59) can be rewritten as

$$\dot{V}(t) + pV(t) \leq q. \tag{60}$$

Multiplying both sides of (60) by the integrating factor e^{pt} yields

$$e^{pt} \dot{V}(t) + pe^{pt} V(t) \leq qe^{pt}. \tag{61}$$

Noting that

$$\frac{\mathrm{d}}{\mathrm{d}t} \left(e^{pt} V(t) \right) = e^{pt} \dot{V}(t) + pe^{pt} V(t), \tag{62}$$

inequality (61) becomes

$$\frac{\mathrm{d}}{\mathrm{d}t} \left(e^{pt} V(t) \right) \leq qe^{pt}. \tag{63}$$

Integrating both sides of (63) over $[0, t]$ gives

$$e^{pt} V(t) - V(0) \leq q \int_0^t e^{ps} \mathrm{d}s = \frac{q}{p} \left(e^{pt} - 1 \right). \tag{64}$$

Dividing both sides of (64) by e^{pt} yields

$$V(t) \leq e^{-pt} V(0) + \frac{q}{p} \left(1 - e^{-pt} \right). \tag{65}$$

Therefore,

$$V(t) \leq \max\left\{ V(0), \frac{q}{p} \right\}, \tag{66}$$

which proves that $V(t)$ is uniformly bounded. Moreover,

$$\limsup_{t \to \infty} V(t) \leq \frac{q}{p}, \tag{67}$$

which indicates that $V(t)$ is uniformly ultimately bounded.

The inequality above is obtained by adding the four recursive derivative bounds. In this summation, the coupling terms cancel as

$$\frac{1}{2}\xi_2^2 - \frac{1}{2}\xi_2^2 + \frac{1}{2}\xi_3^2 - \frac{1}{2}\xi_3^2 + \frac{1}{2}\xi_4^2 - \frac{1}{2}\xi_4^2 = 0. \tag{68}$$

Hence, the coupling term produced in each recursive step is handled by the subsequent step. Since $V(t)$ is bounded, all error variables ξ_i and parameter-estimation errors $\tilde{\theta}_i$ are bounded. Because each ideal parameter θ_i is a finite constant and $\hat{\theta}_i = \theta_i - \tilde{\theta}_i$, all adaptive estimates $\hat{\theta}_i$ are also bounded.

The boundedness of ξ_1 gives the inverse relation

$$\lambda(t) = \frac{2\varpi(t)}{\pi}\arctan(\xi_1(t)). \tag{69}$$

Since $|\arctan(\xi_1)| < \pi/2$ for every bounded ξ_1, it follows that

$$|\lambda(t)| < \varpi(t). \tag{70}$$

For $t \geq T_f$, $v(t) = 0$ and therefore $\varpi(t) = \lambda(\rho(t))$. Thus,

$$|\tanh(e_1(t))| < \tanh(\rho(t)), \qquad t \geq T_f. \tag{71}$$

Because $\tanh(\cdot)$ is odd and strictly increasing,

$$-\rho(t) < e_1(t) < \rho(t), \qquad t \geq T_f. \tag{72}$$

Therefore, the speed tracking error enters the prescribed performance region after the initial expansion stage and remains within it.

On the finite interval $[0, T_f]$, the initial conditions are finite, and the functions in the closed-loop system are smooth inside the transformed feasible region. Hence, the closed-loop signals remain finite on this compact interval. For $t \geq T_f$, the boundedness of e_1 shown above implies that $\lambda_{e_1} = 1 - \lambda^2$ is bounded away from zero. Since $\varpi(t) = \lambda(\rho(t)) > 0$ and ξ_1 is bounded, both R and $1/R$ are bounded.

The boundedness of the remaining closed-loop signals then follows recursively from the coordinate transformations. In particular, $x_1 = e_1 + y_r, x_2 = \xi_2 + \alpha_1, x_3 = \xi_3 + y_d$, $x_4 = \xi_4 + \alpha_3$. Since the reference signals and their required derivatives are bounded and the RBF basis functions are bounded, the virtual control laws α_1 and α_3, the motor states x_i, and the actual control inputs u_q and u_d are bounded. This completes the proof.

4. Simulation

In this section, a speed tracking simulation is conducted to evaluate the effectiveness of the proposed controller. The simulation is designed to emulate the speed regulation process in asynchronous motor drive systems, especially the start-up, acceleration, and deceleration processes relevant to electric-vehicle propulsion.

The simulation study is organized in four stages. First, the basic tracking performance and boundedness of the internal signals are verified. Second, different initial motor speeds are tested to examine whether the prescribed performance bound can be selected independently of the initial speed tracking error. Third, the performance is evaluated under the considered sensor-fault model. Finally, a comparative simulation under load disturbance is used to quantify the performance improvement over the reference method.

Based on Ref. [23], the parameters of the motor are chosen as $n_p = 1$, $L_m = 0.068$ H, $J = 0.0586\ \mathrm{kg}\cdot\mathrm{m}^2$, $L_s = L_r = 0.0699$ H, $R_r = 0.15\ \Omega$, and $R_s = 0.1\ \Omega$. The load torque is defined as

$$T_L = \begin{cases} 0.1N(0,1) + 0.1\sin(t), & 0 < t \le 3, \\ -0.1U(-1,1) - 0.1\sin(t), & 3 < t \le 5. \end{cases} \mathrm{N}\cdot\mathrm{m}, \quad t \text{ in s.} \tag{73}$$

where $N(0,1)$ is standard Gaussian noise and $U(-1,1)$ is uniform random noise over $[-1,1]$. The reference speed trajectory is designed as

$$y_r = \begin{cases} 30 + 10\sin(t), \\ 35 + 8\sin(t) \end{cases} \mathrm{rad/s}. \tag{74}$$

The selected piecewise sinusoidal reference speed represents acceleration and deceleration commands in electric-vehicle traction operation. Because its slope changes with time, this trajectory can test both transient performance, such as tracking-error peak and convergence speed, and steady-state tracking accuracy.

The controller parameters are selected as follows: $c_1 = 4$, $c_2 = 4$, $c_3 = 70$, $c_4 = 200$, $r_1 = r_2 = r_3 = r_4 = 5$, $a_1 = a_2 = a_3 = a_4 = 10$, $\tau_1 = \tau_2 = \tau_3 = \tau_4 = 1$, and $[x_1(0), x_2(0), x_3(0), x_4(0)]^{\mathrm{T}} = [20, 0, 0.1, 0]^{\mathrm{T}}$. The prescribed performance function is designed as

$$\rho(t) = \begin{cases} 0.6\left(1 - \dfrac{t}{0.4}\right)\exp\left(1 - \dfrac{0.4}{0.4-t}\right) + 0.05, & t < 0.4, \\ 0.05, & t \ge 0.4. \end{cases} \tag{75}$$

In the RBFNN, the centers of the receptive fields are $\mu_i = [-1.5, -1, -0.5, 0, 0.5, 1, 1.5, 2]^{\mathrm{T}}$, $o_i = 2$, and $i = 1, 2, 3, 4$.

The baseline simulation results are shown in Figures 1–5. The pink dashed boxes and their associated arrows denote the local zoom-in views of the corresponding regions. Figure 1 presents the motor speed tracking response x_1 and the reference trajectory y_r. The results demonstrate that the proposed controller can accurately follow speed commands, which is essential for maintaining dynamic performance in electric vehicle drive systems. The two trajectories are almost coincident, indicating the ability of the proposed controller to achieve accurate tracking.

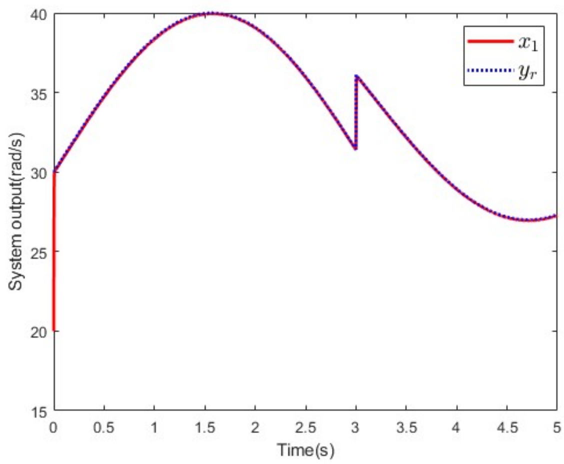

Figure 1. Motor speed tracking response x_1 and reference speed y_r (rad/s).

Figure 2 shows the tracking error e and the prescribed performance boundary ρ. The tracking error initially lies outside the prescribed boundary, but it enters the prescribed region before the specified settling time. This result shows that the prescribed performance bound can be selected independently of the initial speed tracking error, which is important under sensing uncertainty.

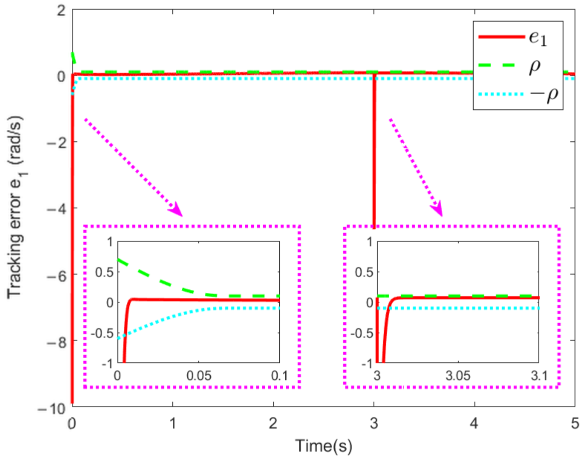

Figure 2. Speed tracking error e_1 and prescribed performance boundary ρ (rad/s).

Figure 3 shows that the rotor flux linkage and d-q-axis currents remain bounded. Figure 4 shows that the control voltage inputs are bounded. Figure 5 confirms that the adaptive estimates also remain bounded.

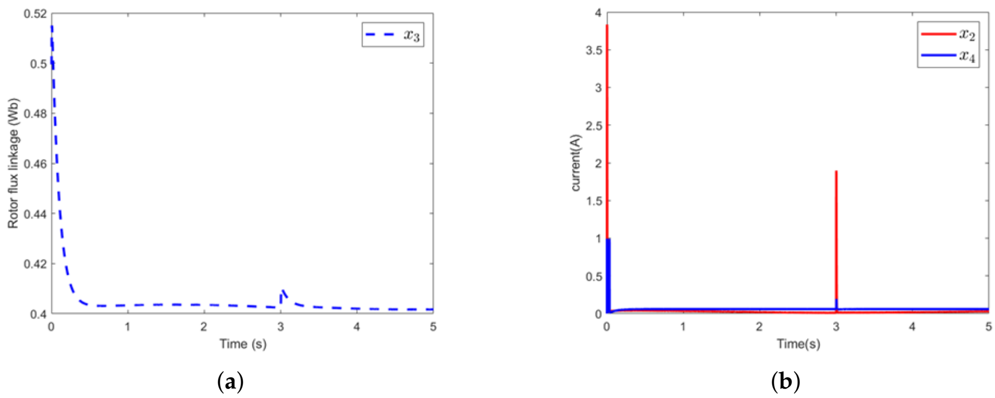

Figure 3. Internal motor states: (**a**) rotor flux linkage x_3 (Wb); (**b**) q-axis current x_2 and d-axis current x_4 (A).

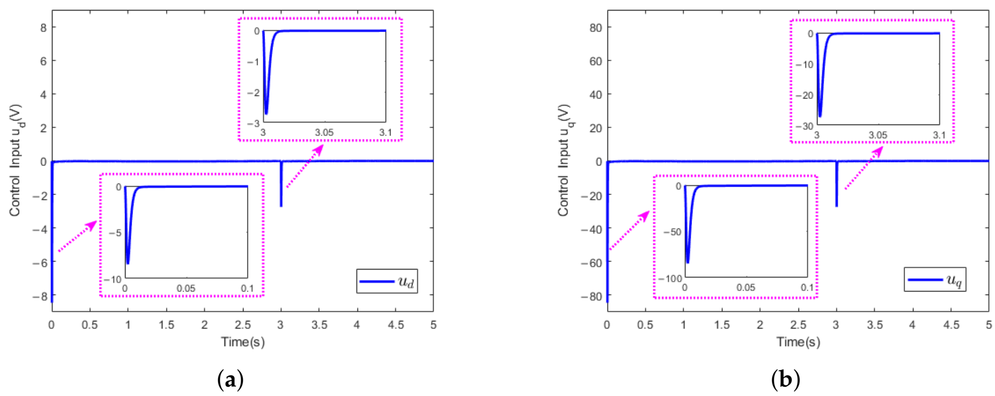

Figure 4. Control voltage inputs: (**a**) u_d and (**b**) u_q (V).

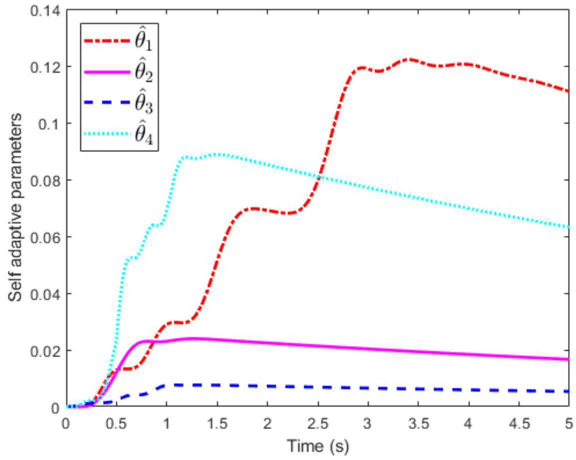

Figure 5. Adaptive parameter estimates used in the four adaptive laws.

Figures 1–5 demonstrate that all internal signals remain bounded, thereby confirming the boundedness result proven in Section 3.2.

To verify that the proposed method does not require the initial speed tracking error to satisfy the prescribed bounds, simulations are conducted with three different initial motor speeds, defined as follows:

- Case 1: $[x_1(0), x_2(0), x_3(0), x_4(0)] = [40, 0, 0.1, 0]$;
- Case 2: $[x_1(0), x_2(0), x_3(0), x_4(0)] = [50, 0, 0.1, 0]$;
- Case 3: $[x_1(0), x_2(0), x_3(0), x_4(0)] = [10, 0, 0.1, 0]$.

In this simulation, all system parameters remained the same, except for the initial motor speed. The tracking errors are shown in Figure 6, which reveals that the prescribed performance can be achieved under different initial motor speeds, indicating that the prescribed performance design is independent of the initial speed tracking error.

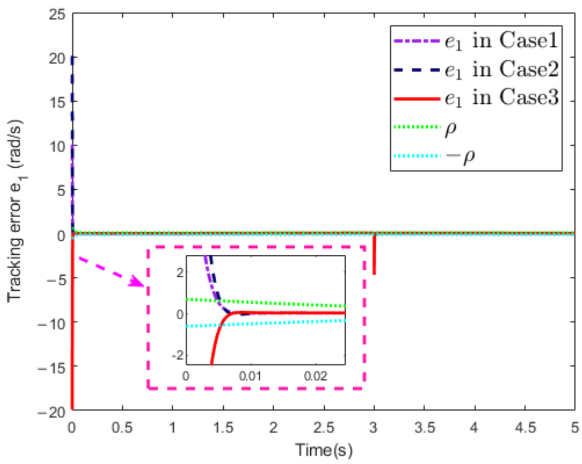

Figure 6. Tracking errors under different initial motor speeds (Cases 1–3).

To evaluate the performance of the proposed controller under measurement uncertainty in practical electric drive applications, the considered sensor-fault model is adopted [23]. Such sensing uncertainties may arise from sensor aging, electromagnetic interference, communication disturbances, or harsh operating environments in electric vehicle drive systems. The measured signal y_{mea} is expressed as

$$y_{\text{mea}} = \Xi_G y + \Xi_B, \tag{76}$$

where $\Xi_G = 0.5$ represents gain fault, and Ξ_B denotes bias fault. Specifically, Ξ_B is constructed as $\Xi_B = 0.5N(0,1) + 0.5U(-1,1)$, The simulation results are shown in Figure 7. It can be observed that, despite the presence of gain error, bias error, and measurement noise, satisfactory tracking performance is maintained under the considered sensor-fault conditions. The tracking error remains within the prescribed performance bounds after a short transient phase, and no significant oscillations are observed.

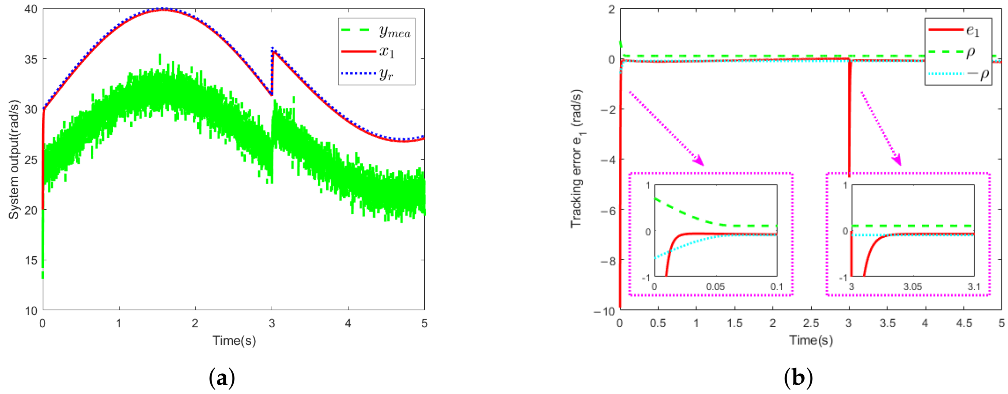

Figure 7. Tracking performance under sensor fault conditions: (**a**) motor speed output and reference speed; (**b**) tracking error.

Note: Convergence time is defined as the first time at which the tracking error enters and remains within the prescribed performance bound before the load disturbance. The steady-state error is calculated as the mean absolute tracking error over the final 0.5 s of the simulation. The maximum tracking error is the maximum positive tracking-error peak after the first zero crossing. The recovery time is the time required for the tracking error to re-enter and remain within the prescribed performance bound after the load disturbance at t = 3 s.

To evaluate the advantages of the proposed method, a comparative simulation with the adaptive controller in Ref. [25] was performed. In this simulation, to evaluate the robustness of the controller, the load torque is defined as

$$T_L = \begin{cases} 1.5 + 0.5\sin(t), & 0 < t \leq 3, \\ -1 + 0.3\sin(t), & 3 < t \leq 5. \end{cases} \mathrm{N}\cdot\mathrm{m}, \quad t \text{ in s.} \tag{77}$$

The model perturbation

$$d_L = \begin{cases} 0.5 + 0.3U(-1,1), & 2i \leq t < 2i+1, \\ -0.3 + 0.1U(-1,1), & 2i+1 \leq t < 2i+2, \end{cases} \mathrm{N}\cdot\mathrm{m}, \quad t \text{ in s} \quad i = 0,1,2,\ldots \tag{78}$$

is introduced into the motor model. Accordingly, the third equation in (1) is rewritten as

$$\dot{x}_3 = x_4 + F_3 + d_L. \tag{79}$$

The other parameters were the same as those used in a previous case.

Figure 8 compares the tracking errors. Table 1 presents a quantitative comparison between the proposed method and the method in Ref. [25]. Compared with Ref. [25], the proposed method reduces the convergence time, steady-state error, and maximum tracking error by 69.5%, 93.4%, and 92.2%, respectively. After the disturbance is applied, the proposed method returns to the specified error range more rapidly, with a 49.4% shorter recovery time. These results indicate that the proposed method provides faster convergence, higher steady-state accuracy, a smaller maximum tracking error, and better disturbance-recovery performance.

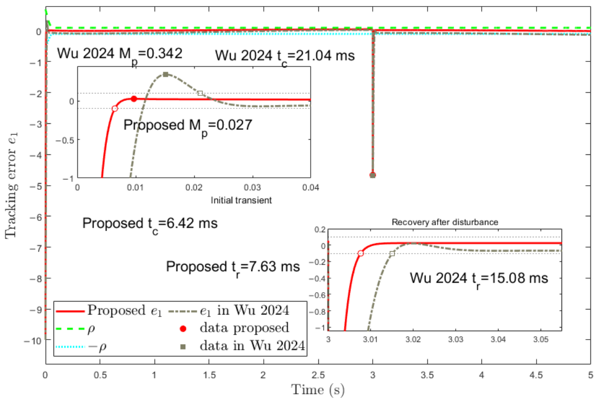

Figure 8. Tracking-error comparison between the proposed method and the method in [25] under load disturbance.

Table 1. Performance comparison of tracking-error metrics for e_1.

Metric	Proposed Method	Method in Ref. [25]	Improvement
Convergence time (s)	0.00642	0.02104	69.5
Steady-state error (rad/s)	0.00697	0.10505	93.4
Maximum tracking error (rad/s)	0.02685	0.34216	92.2
Recovery time after disturbance (s)	0.00763	0.01508	49.4

5. Conclusions

In this study, an adaptive PPC method was developed for asynchronous motor speed regulation. A nonlinear mapping and an improved tangent-type BLF were used to remove the restriction that the initial tracking error must lie within the prescribed performance bounds. Therefore, the prescribed performance function can be selected independently of the initial motor speed. The stability analysis showed that all closed-loop signals remain bounded and that the tracking error enters and remains within the prescribed performance region after the initial expansion stage.

Simulations with different initial motor speeds, the considered sensor-fault model, and load disturbances verified the effectiveness of the proposed method. Under the adopted comparative conditions, the proposed method reduced the convergence time, steady-state error, maximum tracking error, and recovery time by 69.5%, 93.4%, 92.2%, and 49.4%, respectively, compared with the reference method. These results show that the proposed controller provides faster response, higher tracking accuracy, and better recovery after disturbance. However, the proposed method has only been verified through numerical simulations, and the considered disturbance and sensor-fault models are relatively simple. Future work will focus on experimental validation under more realistic disturbances, sensor faults, parameter variations, and input constraints.

Author Contributions: Methodology, R.S. and S.H.; Validation, Z.Z. (Zishuo Zhao); Formal analysis, S.H.; Investigation, S.H.; Data curation, S.H. and Z.Z. (Zishuo Zhao); Writing—original draft, R.S. and Y.Z.; Writing—review & editing, N.S., S.H. and Z.Z. (Zishuo Zhao); Visualization, Z.Z. (Zhongyu Zhang) and Z.Z. (Zishuo Zhao). All authors have read and agreed to the published version of the manuscript.

Funding: This work was supported by the National Natural Science Foundation of China (52201258), the Natural Science Foundation of Jiangsu Province (BK20210650, BK20210651)

Data Availability Statement: The original contributions presented in this study are included in the article. Further inquiries can be directed to the corresponding authors.

Acknowledgments: All authors thank X. Li for her continuous support at the time of writing this paper. All authors thank the Preliminary Research Project on Leading Technologies by Wuxi Industrial Innovation Research Institute.

Conflicts of Interest: The author Ye Zhang was employed by the company Sinopec Yangzi Petrochemical Co., Ltd. The remaining authors declare that the research was conducted in the absence of any commercial or financial relationships that could be construed as a potential conflict of interest.

Abbreviations

The following abbreviations are used in this manuscript:

PID	proportional–integral–derivative
SMC	sliding mode control
BLF	barrier Lyapunov function
PPC	prescribed performance control
RBFNN	radial basis function neural network

References

1. Feng, R.; Hua, Z.; Yu, J.; Zhao, Z.; Dan, Y.; Zhai, H.; Shu, X. A Comparative Investigation on the Energy Flow of Pure Battery Electric Vehicle under Different Driving Conditions. *Appl. Therm. Eng.* **2025**, *269*, 126035. [CrossRef]
2. Xie, F.; Qiu, C.; Qian, Z. Optimal Speed–Torque Control of Asynchronous Motor for Electric Cars in the Field-Weakening Region Based on Voltage Vector Optimization. *IEEE Trans. Power Electron.* **2022**, *37*, 830–842. [CrossRef]
3. Gao, Z.; Zhang, Y.; Guo, G. Finite-Time Fault-Tolerant Prescribed Performance Control of Connected Vehicles with Actuator Saturation. *IEEE Trans. Veh. Technol.* **2023**, *72*, 1438–1448. [CrossRef]
4. Chantoufi, A.; Derouich, A.; El Ouanjli, N.; Mahfoud, S.; El Idrissi, A.; Tazay, A.F.; Mosaad, M.I. Direct Torque Control-Based Backstepping Speed Controller of Doubly Fed Induction Motors in Electric Vehicles: Experimental Validation. *IEEE Access* **2024**, *12*, 139758–139772. [CrossRef]
5. Oguz, Y.; Dede, M. Speed Estimation of Vector Controlled Squirrel Cage Asynchronous Motor with Artificial Neural Networks. *Energy Convers. Manag.* **2011**, *52*, 675–686. [CrossRef]
6. Tepljakov, A.; Gonzalez, E.A.; Petlenkov, E.; Belikov, J.; Monje, C.A.; Petras, I. Incorporation of Fractional-Order Dynamics into an Existing PI/PID DC Motor Control Loop. *ISA Trans.* **2016**, *60*, 262–273. [PubMed]
7. El Daoudi, S.; Lazrak, L.; Ait Lafkih, M. Sliding Mode Approach Applied to Sensorless Direct Torque Control of Cage Asynchronous Motor via Multi-Level Inverter. *Prot. Control Mod. Power Syst.* **2020**, *5*, 13. [CrossRef]
8. Yang, T.; Deng, Y.; Li, H.; Sun, Z.; Cao, H.; Wei, Z. Fast Integral Terminal Sliding Mode Control with a Novel Disturbance Observer Based on Iterative Learning for Speed Control of PMSM. *ISA Trans.* **2023**, *134*, 460–471. [PubMed]
9. Zhang, L.; Tao, R.; Zhang, Z.-X.; Chien, Y.-R.; Bai, J. PMSM Non-Singular Fast Terminal Sliding Mode Control with Disturbance Compensation. *Inf. Sci.* **2023**, *642*, 119040. [CrossRef]
10. Xu, Z.; Sun, C.; Liu, Q. Output-Feedback Prescribed Performance Control for the Full-State Constrained Nonlinear Systems and Its Application to DC Motor System. *IEEE Trans. Syst. Man Cybern. Syst.* **2023**, *53*, 3898–3907. [CrossRef]
11. Madariaga, C.; Gallardo, C.; Reyes, N.; Tapia, J.A.; Jara, W.; Degano, M. Design and Evaluation of Matrix Rotor Induction Motor for High-Torque Low-Speed Applications. *IEEE Trans. Energy Convers.* **2025**, *40*, 295–305. [CrossRef]
12. Wang, S.; Chen, Q. RISE-Based Prescribed Performance Control for Multimotor Driving Systems. *IEEE Trans. Ind. Inform.* **2025**, *21*, 5471–5479. [CrossRef]
13. Liu, L.; Liu, P.; Teng, Z.; Zhang, L.; Fang, Y. Predefined-Time Position Tracking Optimization Control with Prescribed Performance of the Induction Motor Based on Observers. *ISA Trans.* **2024**, *147*, 187–201. [CrossRef] [PubMed]
14. Xu, Z. RISE-Based Asymptotic Adaptive Prescribed Performance Control of Uncertain Nonlinear Systems and Application to DC Motor. *Eur. J. Control* **2025**, *81*, 101168. [CrossRef]
15. Shao, N.; Wu, S.; Zhang, L.; Liu, L.; Fang, Y. Adaptive Observers-Based Fixed-Time Prescribed Performance Position Tracking Optimisation Control for the Induction Motor. *Int. J. Control* **2025**, *98*, 2410–2428.

16. Liu, Y.; Liu, X.; Jing, Y. Adaptive Neural Networks Finite-Time Tracking Control for Non-Strict Feedback Systems via Prescribed Performance. *Inf. Sci.* **2018**, *468*, 29–46. [CrossRef]
17. Liu, B.; Hou, M.; Ni, J.; Li, Y.; Wu, Z. Asymmetric Integral Barrier Lyapunov Function-Based Adaptive Tracking Control Considering Full-State with Input Magnitude and Rate Constraint. *J. Frankl. Inst.* **2020**, *357*, 9709–9732. [CrossRef]
18. Li, Y.-X. Command Filter Adaptive Asymptotic Tracking of Uncertain Nonlinear Systems with Time-Varying Parameters and Disturbances. *IEEE Trans. Autom. Control* **2022**, *67*, 2973–2980. [CrossRef]
19. Li, Y.-X. Barrier Lyapunov Function-Based Adaptive Asymptotic Tracking of Nonlinear Systems with Unknown Virtual Control Coefficients. *Automatica* **2020**, *121*, 109181. [CrossRef]
20. Liu, H.; Li, X. A Prescribed-Performance-Based Adaptive Finite-Time Tracking Control Scheme Circumventing the Dependence on the System Initial Condition. *Appl. Math. Comput.* **2023**, *448*, 127912. [CrossRef]
21. Zhai, D.; An, L.; Li, X.; Zhang, Q. Adaptive Fault-Tolerant Control for Nonlinear Systems with Multiple Sensor Faults and Unknown Control Directions. *IEEE Trans. Neural Netw. Learn. Syst.* **2018**, *29*, 4436–4446. [CrossRef] [PubMed]
22. Li, D.; Han, H.-G.; Qiao, J.-F. Fuzzy-Approximation Adaptive Fault Tolerant Control for Nonlinear Constraint Systems with Actuator and Sensor Faults. *IEEE Trans. Fuzzy Syst.* **2024**, *32*, 2614–2624. [CrossRef]
23. Yang, Y.; Shen, Q. Predetermined Performance Fault-Tolerant Control for Vehicle Platoon Against Measurement Drifts and Multiple Input Constraints. *IEEE Trans. Ind. Electron.* **2025**, *72*, 3008–3016. [CrossRef]
24. Wang, X.; Ye, D.; Zhang, L.; Zhao, X. Prescribed Performance Tracking Control for Nonlinear Multiagent Systems with Distributed Observation Errors Compensation. *IEEE Trans. Autom. Sci. Eng.* **2025**, *22*, 5182–5192. [CrossRef]
25. Wu, Q.; Sun, N.; Yang, T.; Fang, Y. Deep Reinforcement Learning-Based Control for Asynchronous Motor-Actuated Triple Pendulum Crane Systems with Distributed Mass Payloads. *IEEE Trans. Ind. Electron.* **2024**, *71*, 1853–1862. [CrossRef]